

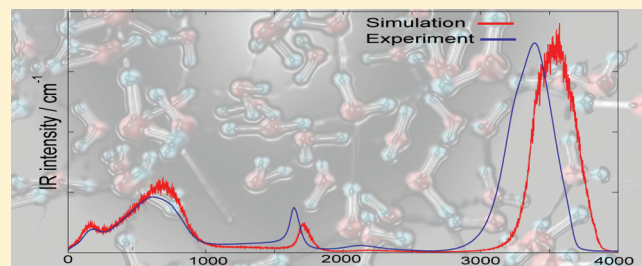
A Polarizable Water Model for Intramolecular and Intermolecular Vibrational Spectroscopies

Taisuke Hasegawa and Yoshitaka Tanimura*

Department of Chemistry, Graduate School of Science, Kyoto University, Kyoto 606-8502, Japan

Supporting Information

ABSTRACT: We have developed a polarizable water model for classical molecular dynamics simulations of vibrational spectroscopies, which covers from low-frequency intermolecular modes to high-frequency intramolecular vibrational modes. The model utilizes the *ab initio* derived geometry-dependent multipole moment surfaces to depict the instantaneous charge density of a water molecule. Multipoles up to quadrupole are included for the permanent multipoles, while those up to dipole are included for the induced multipoles. The polarization of molecules is described by a distributed polarizability model. At room temperature, the present model is able to reproduce experimental infrared and Raman spectra of intramolecular vibrational modes, except for the blue peak shift due to a limitation of the classical simulation based on a quantum mechanical potential. The calculated infrared spectrum for low-frequency intermolecular modes agreed reasonably well with the experimental signals.



1. INTRODUCTION

Molecular dynamics (MD) simulation is a powerful means to analyze optical spectra such as infrared (IR) and Raman spectra, since we can monitor molecular motions and manipulate physical conditions in a variety of ways. However, the applicability of MD is limited by CPU power due to the numerous molecular degrees of freedom for a system in condensed phase. In such a case, a full quantum simulation is not affordable and one has to treat the molecular motions and interactions classically. Taking advantage of easy-to-use classical dynamical formulations and classical interaction potentials, one can calculate linear and nonlinear optical spectra defined by the response functions of the dipole moment or polarizability of the total system.¹ While this approach is handy, it is phenomenological; molecular interactions inherently arise from the interactions between the atoms and their surrounding electrons; however, classical MD simulations replace these interactions by empirical potentials to reproduce either experimental results or *ab initio* electronic structure calculations.

Among the molecular liquids, water is of great interest due to its many unusual properties² and its important role in biology and chemistry. Numerous studies of optical spectra of liquid water have been carried out by computer simulations with various methods including MD.^{3–17} A tremendous effort has been made to create potential models to account for IR and Raman spectra of liquid water. Because the dipole moment and polarizability of a water molecule are sensitive to its environment, their evaluation is a delicate issue when one simulates the optical properties of liquid water by means of MD simulations. The dipole moment and polarizability are functions of the instantaneous charge density and its response with respect to the electric fields; therefore, the optimal choice may be an appropriately

constructed “on the fly” *ab initio* MD (AIMD) simulation.^{18,19} Since this simulation can intrinsically duplicate the instantaneous charge densities of water molecules in the liquid phase and is generally suitable for simulating optical spectra, many AIMD studies of water or deuterated water have been conducted.^{5,20–23} If the computationally expensive MD simulations were to be conducted for simulating optical responses, one could utilize an empirical water model as an alternative choice, since simulating two-dimensional IR (2DIR) spectra²⁴ by means of AIMD simulations is not feasible with typical computational resources.

We have therefore attempted to develop an empirical water model for simulating the optical spectra for liquid water. To reproduce experimental IR and Raman spectra of bulk water, the water model needs to have the appropriate many-body electronic polarization effects, accurate inter- and intramolecular potential energy surfaces (PESs), and an accurate monomer dipole moment surface (DMS). There are many techniques to make an empirical potential model polarizable. Among them, the fluctuating charge model,^{25–27} the Thole type dipole polarizability model,^{28,29} and the charge response kernel model^{30–32} have been widely used to handle the polarization effect. Many polarizable water potentials have been developed, each with various strengths.³³ For example, the POLS/TZ and POLS/QZ water models handle the polarization effect via fluctuating charges and induced dipole moments.³⁴ The AMOEBA and AMOEBA- ν

Special Issue: Shaul Mukamel Festschrift

Received: November 29, 2010

Revised: March 3, 2011

Published: April 12, 2011

water models employ the dipole-polarizability model.^{35,36} These polarizable potential models can reproduce the experimental properties of liquid water well; however, they are either rigid models or do not have accurate intramolecular monomer PES and DMS, and so cannot reproduce intramolecular IR spectra so well.

Accurate intramolecular monomer PES and DMS of water monomer were developed by Partridge and Schwenke (PS).³⁷ Also developed recently are the flexible, polarizable Thole-type model version III (TTM3F)³⁸ and the flexible polarizable Thole-type model version IV (TTM4F)³⁹ potentials for IR spectra, which utilize the Thole-type dipole polarization model, PS's intramolecular PES, and PS's monomer DMS. Those potentials almost correctly describe the IR line shape and intensity of the OH stretching vibration band obtained from experiments. However, the validity of the combination of the separately developed polarization model and monomer DMS is unclear. The polarizable, flexible, and transferable potential for water (POLIR) potential⁴⁰ uses only PS's PES. This potential model has polarization and a nonlinear DMS, both of which are empirically parametrized for consistency. The POLIR model shows good agreement with the experimental IR spectrum of the OH stretching band; however, it does not reproduce the experimental oxygen–oxygen radial distribution function (RDF).⁴⁰ Various techniques to calculate linear and multidimensional vibrational spectra, such as two-dimensional (2D) Raman⁴¹ and 2D IR⁴² spectra, have also been suggested and examined.^{12,43–53} Since multidimensional vibration spectra are more sensitive to the classical force field than linear spectra,⁵⁴ it is important to develop a precise potential which covers inter- and intramolecular vibrational motions.

In this study, we present a polarizable water model for inter- and intramolecular vibrational spectroscopy (POLI2VS) based on the POLIR potential. The DMS and the polarization effect were implemented by means of the distributed multipole analysis (DMA)⁵⁵ and the distributed polarization model⁵⁶ to describe the instantaneous charge density of a water molecule in a consistent way. In order to reproduce the structure of liquid water, multipoles up to quadrupole are used for the permanent part and multipoles up to dipole are used for the induced part. While we constructed the present water model with a consistent treatment of the DMS and the polarization effect so as to reproduce the experimental IR spectra of the OH stretching mode,⁵⁷ the present model also reproduces Raman spectra⁵⁸ reasonably well. Although the capability of describing low-frequency Raman spectra is limited, the present model can also accurately describe low-frequency IR spectra corresponding to intermolecular vibrational motions. Thus, the present model provides a unified description of low-frequency intermolecular to high-frequency intramolecular modes.

This paper is organized as follows. In section 2, our water potential model is introduced and explained. In section 3, we present some calculated properties of bulk water. In sections 4 and 5, IR and Raman spectra are discussed. Section 6 is devoted to concluding remarks.

2. A POLARIZABLE WATER MODEL FOR INTER- AND INTRAMOLECULAR VIBRATIONAL SPECTROSCOPY (POLI2VS)

A. Potential Function. The total potential energy of the water model is written as

$$U = U_{\text{elec}} - U_{\text{elec, monomer}} + U_{\text{ind}} - U_{\text{ind, monomer}} + U_{\text{nonelec}} + U_{\text{intra}} \quad (1)$$

where U_{elec} , $U_{\text{elec, monomer}}$, U_{ind} , $U_{\text{ind, monomer}}$, U_{nonelec} , and U_{intra} are the electrostatic energy of bulk water, the electrostatic energy of isolated water molecules, the induction energy of bulk water, the induction energy of isolated water molecules, the repulsion–dispersion energy, and the intramolecular bonding energy, respectively. When we employ the distributed multipoles, the electrostatic energy is composed of multipole interaction energies as

$$U_{\text{elec}} = U_{\text{CC}} + U_{\text{CD}} + U_{\text{DD}} + U_{\text{CQ}} + U_{\text{DQ}} + U_{\text{QQ}} \quad (2)$$

where the subscripts CC, CD, DD, CQ, DQ, and QQ stand for charge–charge, charge–dipole, dipole–dipole, charge–quadrupole, dipole–quadrupole, and quadrupole–quadrupole, respectively. The multipole interaction energy of isolated water molecules is expressed as

$$U_{\text{elec, monomer}} = U_{\text{CD, monomer}} + U_{\text{DD, monomer}} \quad (3)$$

We assume that there is an electrostatic interaction site on each atom; that is to say, a water molecule has three interaction sites. We will let i and j denote the indices of atomic interaction sites and α and β denote the indices of water molecules. The multipole interactions in the short-range region are screened by damping functions in order to avoid a “polarization catastrophe”.²⁹ Introducing the damping functions, the screened multipole interactions are written as

$$U_{\text{CC}} = \sum_{\alpha} \sum_{\beta > \alpha} \sum_{ij} \frac{q_{\alpha i} q_{\beta j} \lambda_1^{\text{inter}}(R_{\alpha\beta}^{ij})}{R_{\alpha\beta ij}} \quad (4)$$

$$U_{\text{CD}} = \sum_{\alpha} \sum_{\beta \neq \alpha} \sum_{ij} \frac{q_{\alpha i} (\boldsymbol{\mu}_{\beta j} \cdot \mathbf{R}_{\alpha\beta ij})}{R_{\alpha\beta ij}^3} \lambda_3^{\text{inter}}(R_{\alpha\beta}^{ij}) + \sum_{\alpha} \sum_i \sum_{j \neq i} \left\{ \frac{q_{\alpha i}^{\text{perm}} (\boldsymbol{\mu}_{\alpha j}^{\text{ind}} \cdot \mathbf{R}_{\alpha\alpha ij})}{R_{\alpha\alpha ij}^3} \right\} \lambda_3^{\text{intra}}(R_{\alpha\alpha}^{ij}) \quad (5)$$

$$U_{\text{DD}} = \sum_{\alpha} \sum_{\beta > \alpha} \sum_{ij} \left(\frac{\boldsymbol{\mu}_{\alpha i} \cdot \boldsymbol{\mu}_{\beta j}}{R_{\alpha\beta ij}^3} \lambda_3^{\text{inter}}(R_{\alpha\beta}^{ij}) - \frac{3(\boldsymbol{\mu}_{\alpha i} \cdot \mathbf{R}_{\alpha\beta ij})(\boldsymbol{\mu}_{\beta j} \cdot \mathbf{R}_{\alpha\beta ij})}{R_{\alpha\beta ij}^5} \lambda_5^{\text{inter}}(R_{\alpha\beta}^{ij}) \right) + \sum_{\alpha} \sum_i \sum_{j > i} \left(\frac{\boldsymbol{\mu}_{\alpha i} \cdot \boldsymbol{\mu}_{\alpha j}}{R_{\alpha\alpha ij}^3} \lambda_3^{\text{intra}}(R_{\alpha\alpha}^{ij}) - \frac{3(\boldsymbol{\mu}_{\alpha i} \cdot \mathbf{R}_{\alpha\alpha ij})(\boldsymbol{\mu}_{\alpha j} \cdot \mathbf{R}_{\alpha\alpha ij})}{R_{\alpha\alpha ij}^5} \lambda_5^{\text{intra}}(R_{\alpha\alpha}^{ij}) \right) \quad (6)$$

$$U_{\text{CQ}} = \sum_{\alpha} \sum_{\beta \neq \alpha} \sum_{ij} \frac{\mathbf{R}_{\alpha\beta ij} \mathbf{Q}_{\alpha i} \mathbf{R}_{\alpha\beta ij}}{R_{\alpha\beta ij}^5} q_{\beta j} \lambda_5^{\text{inter}}(R_{\alpha\beta}^{ij}) \quad (7)$$

$$U_{\text{DQ}} = \sum_{\alpha} \sum_{\beta \neq \alpha} \sum_{ij} \left(\frac{2\boldsymbol{\mu}_{\alpha i} \mathbf{Q}_{\beta j} \mathbf{R}_{\alpha\beta ij}}{R_{\alpha\beta ij}^5} \lambda_5^{\text{inter}}(R_{\alpha\beta}^{ij}) - \frac{5(\boldsymbol{\mu}_{\alpha i} \cdot \mathbf{R}_{\alpha\beta ij}) \mathbf{R}_{\alpha\beta ij} \mathbf{Q}_{\beta j} \mathbf{R}_{\alpha\beta ij}}{R_{\alpha\beta ij}^7} \lambda_7^{\text{inter}}(R_{\alpha\beta}^{ij}) \right) \quad (8)$$

$$U_{\text{QQ}} = \frac{1}{3} \sum_{\alpha} \sum_{\beta > \alpha} \sum_{ij} \left(\frac{2\text{tr}[\mathbf{Q}_{\alpha i} \mathbf{Q}_{\beta j}]}{R_{\alpha\beta ij}^5} \lambda_5^{\text{inter}}(R_{\alpha\beta}^{ij}) \right. \\ \left. - \frac{20R_{\alpha\beta ij} \mathbf{Q}_{\alpha i} \mathbf{Q}_{\beta j} R_{\alpha\beta ij}}{R_{\alpha\beta ij}^7} \lambda_7^{\text{inter}}(R_{\alpha\beta}^{ij}) \right. \\ \left. + \frac{35(R_{\alpha\beta ij} \mathbf{Q}_{\alpha i} R_{\alpha\beta ij})(R_{\alpha\beta ij} \mathbf{Q}_{\beta j} R_{\alpha\beta ij})}{R_{\alpha\beta ij}^9} \lambda_9^{\text{inter}}(R_{\alpha\beta}^{ij}) \right) \quad (9)$$

where q , q^{perm} , $\boldsymbol{\mu}$, $\boldsymbol{\mu}^{\text{ind}}$, and \mathbf{Q} are the total (permanent + induced) partial charge, the permanent partial charge, the total dipole moment, the induced dipole moment, and the traceless quadrupole,⁵⁹ respectively. $\mathbf{R}_{\alpha\beta ij}$ is a vector from the j th site of the molecule β toward the i th site of the molecule α , $\lambda(u)$ is the damping function and we set $R_{\alpha\beta ij} = |\mathbf{R}_{\alpha\beta ij}|$ and $R_{\alpha\beta}^{ij} = R_{\alpha\beta ij}/A_{ij}$ with a damping parameter A_{ij} . Since an isolated water molecule in the present model contains the unnecessary interaction energy which arises from the intramolecular dipole–dipole and charge–dipole interactions, we subtract the water monomer energies from the total energy following the procedure used in the POLIR potential.⁴⁰

Following Thole's study,²⁹ the first order damping function for intermolecular interactions is expressed as

$$\lambda_1^{\text{inter}}(u) = 1 - \exp[-au^3] + a^{1/3}u\Gamma(2/3)Q(2/3, au^3) \quad (10)$$

where $\Gamma(x)$ is the Gamma function, a is the damping parameter, and $Q(x, y)$ is the incomplete Gamma function. For the intramolecular first order damping function, we adopt the steeper damping function introduced by Burnham, namely,³⁹

$$\lambda_1^{\text{intra}}(u) = 1 - \exp[-au^4] + a^{1/4}u\Gamma(3/4)Q(3/4, au^4) \quad (11)$$

In both cases, the higher order damping functions are evaluated from

$$\lambda_{n+2}(u) = \lambda_n(u) - \frac{u}{n} \frac{d\lambda_n(u)}{du} \quad \text{for } n = 1, 3, 5, \dots \quad (12)$$

Thole originally used isotropic atomic polarizabilities and defined the parameter in the screened multipole interactions as $A_{ij} = (\alpha_i \alpha_j)^{1/6}$. Here, we considered anisotropic atomic polarizabilities on atoms, so that we used the effective isotropic polarizabilities for the damping parameters. We adopt the value of α_{O} and α_{H} as 0.862 and 0.514, respectively.²⁹ The damping parameters a for each multipole interaction are different and are denoted by a^{CC} , a^{CD} , a^{DD} , a^{CQ} , a^{DQ} , and a^{QQ} for the charge–charge, charge–dipole, dipole–dipole, charge–quadrupole, dipole–quadrupole, and quadrupole–quadrupole interactions, respectively. The present model employs the distributed polarizability to deal with the induced charges and the induced dipoles.⁵⁵ The induction energy then arises from both the induced dipoles and the induced charges. Using the prescription of the distributed polarizability model, the induction energy from the induced dipoles is written as

$$U_{\text{ind, dipole}} = \frac{1}{2} \sum_{\alpha} \sum_i \boldsymbol{\mu}_{\alpha, i}^{\text{ind}} (\boldsymbol{\alpha}_{\alpha, i})^{-1} \boldsymbol{\mu}_{\alpha, i}^{\text{ind}} \quad (13)$$

where $\boldsymbol{\alpha}_{i\alpha}$ is an atomic polarizability tensor on the i th atom in the molecule α . The induction energy from the induced charges is written as

$$U_{\text{ind, charge}} = \frac{1}{2} \sum_{\alpha} \sum_i \sum_j q_{\alpha, i}^{\text{ind}} (\boldsymbol{\alpha}_{\alpha, ij}^{\text{C}})^{-1} q_{\alpha, j}^{\text{ind}} \quad (14)$$

where $q_{\alpha, i}^{\text{ind}}$ is an induced charge on the i th atom in the molecule α and $\boldsymbol{\alpha}_{\alpha, ij}^{\text{C}}$ is the charge-flow polarizability of the molecule α . We can

now write the total induction energy as $U_{\text{ind}} = U_{\text{ind, charge}} + U_{\text{ind, dipole}}$. The induced charges and the induced dipoles are determined by the equilibrium conditions $\partial(U_{\text{elec}} + U_{\text{ind}})/\partial\boldsymbol{\mu}_i^{\text{ind}} = 0$, $\partial(U_{\text{elec}} + U_{\text{ind}})/\partial q_i^{\text{ind}} = 0$, and $\sum_i q_{\alpha, i}^{\text{ind}} = 0$. Applying these conditions to eqs 2, 13, and 14, we can obtain the set of linear equations

$$\boldsymbol{\mu}_{\alpha, i}^{\text{ind}} = \boldsymbol{\alpha}_{\alpha, i} \mathbf{E}_{\alpha, i} \quad (15)$$

$$q_{\alpha, i}^{\text{ind}} = \sum_{j=1}^2 \alpha_{\alpha, ij}^{\text{C}} (V_{\alpha, 3} - V_{\alpha, j}) \quad (16)$$

where $\mathbf{E}_{\alpha, i}$ is the local electric field and we choose $V_{\alpha, 3}$ as the local electric potential at the oxygen atom of the molecule α . Since these equations are linear in q^{ind} and $\boldsymbol{\mu}^{\text{ind}}$, we can easily solve them by the conjugate gradient (CG) method. We utilize the extrapolation scheme reported in ref 60 in order to predict the initial estimation of the induced terms for iterations. For the bonding energy U_{intra} we utilize the Partridge–Schwenke (PS) intramolecular potential surface,³⁷ which is accurate enough to depict the intramolecular vibrational dynamics in the gas phase.

For the repulsion–dispersion term, we employ Halgren's buffered 14–7 pairwise potential used in the AMOEBA water potential expressed as^{36,61}

$$U_{\text{nonelec}} = \sum_{\alpha} \sum_{\beta \neq \alpha} \sum_{ij} \varepsilon_{ij} \left(\frac{1 + 0.07}{R_{\alpha\beta ij}/R_{ij}^0 + 0.07} \right)^7 \left(\frac{1 + 0.12}{(R_{\alpha\beta ij}/R_{ij}^0)^7 + 0.12} - 2 \right) \quad (17)$$

where ε_{ij} and R_{ij}^0 are the potential well depth and the minimum energy distance, respectively. The combining rules

$$R_{\text{OH}}^0 = \frac{(R_{\text{HH}}^0)^3 + (R_{\text{OO}}^0)^3}{(R_{\text{HH}}^0)^2 + (R_{\text{OO}}^0)^2} \quad (18)$$

and

$$\varepsilon_{\text{OH}} = \frac{4\varepsilon_{\text{HH}}\varepsilon_{\text{OO}}}{(\varepsilon_{\text{HH}}^{1/2} + \varepsilon_{\text{OO}}^{1/2})^2} \quad (19)$$

were used for the interactions between hydrogen and oxygen atoms.

B. Parameterization. The polarization effect of the present model is described by the distributed polarizability. While inclusion of the response of higher multipoles than dipole moment is feasible to draw the accurate instantaneous multipole surface, they are not included in this model due to the computational cost. Within a linear response, the induced dipoles $\mathbf{M} - \mathbf{M}^{\text{perm}}$ and the external field \mathbf{F} are related by

$$\mathbf{M} - \mathbf{M}^{\text{perm}} = \boldsymbol{\alpha} \mathbf{F} \quad (20)$$

where $\mathbf{M} = [\mathbf{q}, \boldsymbol{\mu}]^{\text{T}}$, $\mathbf{M}^{\text{perm}} = [\mathbf{q}^{\text{perm}}, \boldsymbol{\mu}^{\text{perm}}]^{\text{T}}$, and $\mathbf{F} = [\mathbf{V}, \mathbf{E}]^{\text{T}}$ are vectors consisting of the total charges and total dipoles, the permanent charges and permanent dipoles, and the external electric potentials and external electric fields at each atomic center, respectively. The tensor $\boldsymbol{\alpha}$ is the distributed polarizability.

Note that the charge-dipole cross polarizabilities in a water molecule are ignored in the present model. Equation 20 can therefore be decomposed into dipole and charge parts

$$\begin{pmatrix} q_{\text{H1}}^{\text{ind}} \\ q_{\text{H2}}^{\text{ind}} \end{pmatrix} = \alpha^{\text{c}} \Delta V \\ = \begin{pmatrix} \alpha_{\text{H1,H1}}^{\text{c}} & \alpha_{\text{H1,H2}}^{\text{c}} \\ \alpha_{\text{H2,H1}}^{\text{c}} & \alpha_{\text{H2,H2}}^{\text{c}} \end{pmatrix} \begin{pmatrix} V_{\text{O}} - V_{\text{H1}} \\ V_{\text{O}} - V_{\text{H2}} \end{pmatrix} \quad (21)$$

$$\begin{pmatrix} \mu_{\text{H1}}^{\text{ind}} \\ \mu_{\text{H2}}^{\text{ind}} \\ \mu_{\text{O}}^{\text{ind}} \end{pmatrix} = \alpha^{\text{d}} \mathbf{E} \\ = \begin{pmatrix} \alpha_{\text{H1,H1}}^{\text{d}} & \alpha_{\text{H1,H2}}^{\text{d}} & \alpha_{\text{H1,O}}^{\text{d}} \\ \alpha_{\text{H2,H1}}^{\text{d}} & \alpha_{\text{H2,H2}}^{\text{d}} & \alpha_{\text{H2,O}}^{\text{d}} \\ \alpha_{\text{O,H1}}^{\text{d}} & \alpha_{\text{O,H2}}^{\text{d}} & \alpha_{\text{O,O}}^{\text{d}} \end{pmatrix} \begin{pmatrix} \mathbf{E}^{\text{H1}} \\ \mathbf{E}^{\text{H2}} \\ \mathbf{E}^{\text{O}} \end{pmatrix} \quad (22)$$

Here, the charge flow polarizability α^{c} depends on the configuration of the water molecule. The dipole polarizability α^{d} is the function of the atomic polarizabilities and the dumping parameters via eq 15. The finite field *ab initio* calculations at the CCSD/aug-cc-pVQZ level were performed at 129 different water geometries. The induced partial charges and induced dipoles were then obtained from the GDMA program package⁵⁵ via the DMA. The atomic polarizabilities and intramolecular dumping parameters were determined to reproduce the finite difference of induced dipoles with a least-squares fitting. The charge-flow polarizability was then set to reproduce the molecular polarizability by means of a least-squares fitting. The out-of-plane components of atomic polarizabilities, charge-flow polarizabilities, permanent atomic charges, absolute values of the permanent atomic dipole moments, and atomic quadrupoles are expressed in geometry-dependent forms as

$$f(r_1, r_2, \theta) = \sum_{ijk} c_{ijk} \Delta r_1^i \Delta r_2^j \Delta \theta^k, \\ \Delta r_i = r_i - r_{\text{eq}}, \Delta \theta = \theta - \theta_{\text{eq}} \quad (23)$$

where r_i , θ , r_{eq} and θ_{eq} are the OH bond length, the HOH bend angle, the equilibrium bond length, and the equilibrium bend angle, respectively, and c_{ijk} is a fitting parameter. For the atomic dipole moments, we use

$$\boldsymbol{\mu}^{\text{perm}} = \mu(r_1, r_2, \theta) \frac{\mathbf{v}(\mathbf{r}_1, \mathbf{r}_2)}{|\mathbf{v}(\mathbf{r}_1, \mathbf{r}_2)|} \quad (24)$$

$$\mathbf{v}(\mathbf{r}_1, \mathbf{r}_2) = \sum_{ijk} c_{ijk}^{\text{H1}} \Delta r_1^i \Delta r_2^j \Delta r_{\text{HH}}^k \mathbf{r}_1 + \sum_{ijk} c_{ijk}^{\text{H2}} \Delta r_1^i \Delta r_2^j \Delta r_{\text{HH}}^k \mathbf{r}_2 \quad (25)$$

where \mathbf{r}_i is the OH bond vector, $\Delta r_{\text{HH}} = r_{\text{HH}} - r_{\text{HH,eq}}$ is defined by the distance between hydrogen atoms r_{HH} and the equilibrium distance between hydrogen atoms $r_{\text{HH,eq}}$ and c_{ijk}^{H1} and c_{ijk}^{H2} are fitting parameters, respectively. The quadrupole and polarizability of the oxygen atom are defined in the molecular frame; the Z axis lies along the bisector of the HOH angle; the Y axis is normal to the molecular plane; the X axis is perpendicular to the YZ plane. We use the right-hand system for the molecular frame.

Table 1. Potential Parameters^a

function	parameter	value	unit
buffered 14-7 potential	ϵ_{OO}	0.185	kcal/mol
	ϵ_{HH}	1.45×10^{-3}	kcal/mol
	R_{OO}^0	3.577	Å
	R_{HH}^0	2.2	Å
damping			
	O	α^{O}	0.862
H	α^{H}	0.514	Å ³
intramolecular	a	0.41	
	intermolecular	a^{CC}	0.35
	a^{CD}	0.43	
	a^{DD}	0.43	
	a^{CQ}	0.4	
	a^{DQ}	0.125	
	a^{QQ}	0.25	
multipoles	r_{eq}	0.957228	Å
	$r_{\text{HH,eq}}$	1.51395	Å
	θ_{eq}	104.52	deg

^aThe parameters for potential charge, permanent dipole, unit vector of dipole moment, quadrupole, charge polarizability, and dipole polarizability are presented in the Supporting Information.

These quantities for the hydrogen atoms are defined in the OH frame; the Z axis lies along the OH bond; the X axis is defined on the molecular plane and is perpendicular to the Z axis. The permanent multipoles were determined by a least-squares fit to the 188 points DMA data. The DMA was performed by the GDMA program package.⁵⁵ The *ab initio* charge densities were calculated at the CCSD/aug-cc-pVQZ level by the Gaussian 03 program package.⁶²

Remaining parameters were determined empirically. The elements ϵ_{ij} and R_{ij}^0 in the repulsion–dispersion term were determined to reproduce the experimental density at 298.15 K and the pressure of 1 bar. The intermolecular damping parameters of the screened multipole interactions were determined to reproduce the experimental IR spectrum of the O–H stretching vibrations. The important parameters in this model are listed in Table 1.

3. LIQUID WATER PROPERTIES

A. Computational Details. The MD simulations were carried out with 216 water molecules. The charge–charge, charge–dipole, and dipole–dipole interactions were dealt by the standard EWALD summation with the tinfoil boundary condition, while the interactions involving quadrupoles were cut off with the smoothing function. Note that the normal electrostatic interactions were used in the EWALD summation instead of the screened electrostatic interaction. This treatment is valid because the corrections made by the damping factors affect only short-range interactions.⁶³ As mentioned in section 2, the set of linear equations were solved by the CG method. The convergence criterion was $|\mathbf{r}| < 5 \times 10^{-8}$ eÅ, where the residual vector elements r_i which have the unit of e were multiplied by 1 Å to have the unit of eÅ. For isothermal–isobaric and isothermal simulations, we solved the equations of motion by the explicit reversible integrator⁶⁴ with a time step of 0.1 fs. For microcanonical ensemble (NVE) simulations, we used the RESPA

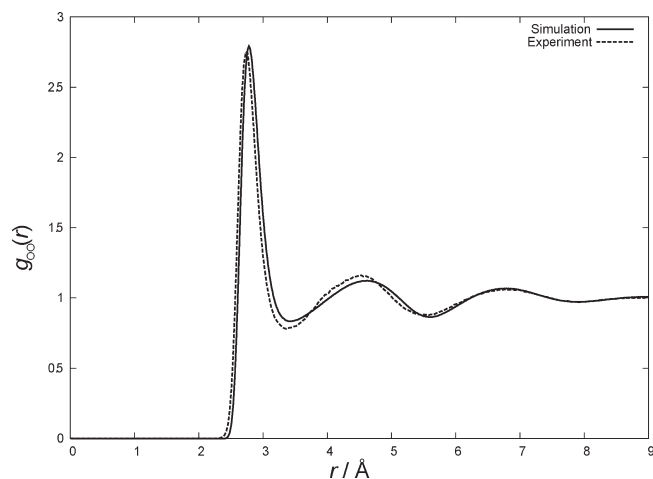


Figure 1. Oxygen–oxygen radial distribution function $g_{\text{OO}}(r)$ at 298.15 K under 1 bar. The experimental data of Soper's group⁶⁷ is also presented as the dashed line for comparison.

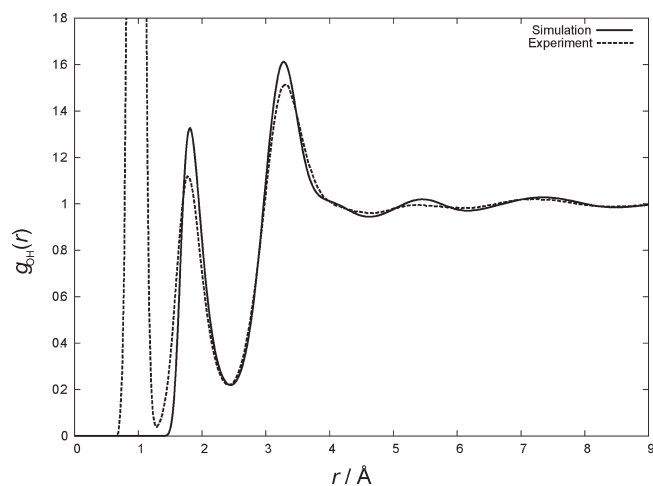


Figure 2. Oxygen–hydrogen radial distribution function $g_{\text{OH}}(r)$ at 298.15 K under 1 bar. The experimental data of Soper's group⁶⁷ is presented as the dashed line for comparison. The intramolecular contribution that appears as the first peak at $r = 1$ of the experimental result does not appear in the simulation.

algorithm,⁶⁵ where the bonded part of the evolution operator was integrated by the sixth order symplectic method, while the others were integrated by the second order method. The simulation box used in constant volume simulations was 18.639 Å on a side. The repulsion–dispersion forces and the electrostatic interactions including quadrupoles were cut off smoothly from 9.0 to 9.1 Å with the smoothing function (see the Appendix). The temperature and pressure of the *NPT* simulations were set at 298.15 K and 1 bar. The temperature of the *NVT* simulations was set at 298.15 K. The *NPT*, *NVT*, and *NVE* ensembles were obtained from separate 32 simulation runs (3.2 ns total simulation time), separate 16 simulation runs (1.6 ns total simulation time), and separate 16 simulation runs (3.2 ns total simulation time), respectively. The IR and Raman spectra were calculated from separate 16 constant energy simulation runs. The total simulation time for simulating the IR and Raman spectra was 3.2 ns. All the simulation runs were carried out after 200 ps equilibration. It

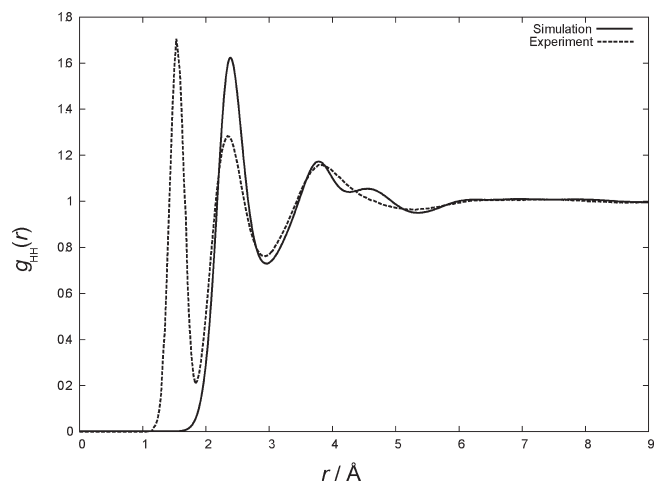


Figure 3. Hydrogen–hydrogen radial distribution function $g_{\text{HH}}(r)$ at 298.15 K under 1 bar. The experimental data of Soper's group⁶⁷ is presented as the dashed line for comparison. The intramolecular contribution that appears as the first peak at $r = 1.5$ of the experimental result does not appear in the simulation.

was found that the computational cost of this model was about 40 times more expensive than that of nonpolarizable models, such as the SPC/E water model.⁶⁶

The standard errors (SEs) of the averaged dynamic properties were estimated from $\text{SE} = \sigma' / (n)^{1/2}$, where σ' is the sample standard deviation of the averaged dynamic properties obtained from the independent MD trajectories and n is the number of independent MD trajectories.

B. Bulk Water Properties. Radial distribution functions (RDFs) at 298.15 K and a pressure of 1 bar were computed from the trajectories of the *NPT* simulations. Unless stated otherwise, all other properties described here were also computed by *NPT* simulations. Figures 1–3 show calculated RDFs and the experimental data obtained by Soper's group.⁶⁷ While the computed oxygen–oxygen RDF ($g_{\text{OO}}(r)$) exhibits a slightly higher first peak and shallower first trough than the experimental data, it is consistent with the experimental results. However, it is necessary to incorporate quantum corrections into MD simulations to properly compare the simulated results with the experimental RDFs. The self-diffusion coefficient was computed from the Einstein relation using the center of mass trajectories in the *NVE* simulations. The slope of the mean-squared displacement was fitted from the range of 10–50 ps data. We obtained a self-diffusion coefficient of about $1.83 \times 10^{-5} \text{ cm}^2/\text{s}$. This is lower than the experimental value of $2.32 \times 10^{-5} \text{ cm}^2/\text{s}$.⁶⁸ In the present model, the angle of the monomer HOH bond is 104.52° at the optimized configuration, while the averaged angle of the HOH bond in liquid water is 105.14° , which is within the error bound of experimental data.⁶⁹ The increase of HOH bond angle in liquid water was first reported with the TTM2-F model,⁷⁰ and has also been reported with the TTM3F, TTM4F, and POLIR models, all of which employ the nonlinear DMS. The average molecular dipole moment in liquid was evaluated as 2.93 D in the present model, while the recently reported experimental value of the average molecular dipole moment is around 2.9 D⁷¹ and the *ab initio* studies including AIMD simulations have reported values of 2.4–3.0 D.^{19,72} The averaged liquid density calculated from the present model at 298.15 K under 1 bar is about $0.993 \text{ g}/\text{cm}^3$, which is slightly lower than the experimental

Table 2. Liquid Water Properties

	unit	the present model	experiment	ensemble
ΔH_{vap}	kcal/mol	10.54 ± 0.01	10.52^a	NPT
E_{liq}	kcal/mol	-9.036 ± 0.006		NPT
E_{gas}	kcal/mol	0.900 ± 0.002		NVT ^f
$\langle \theta_{\text{HOH}} \rangle$	deg	105.139 ± 0.004	106^b	NPT
$\langle r_{\text{OH}} \rangle$	Å	0.97703 ± 0.00003	0.970^b	NPT
ρ	g/cm ³	0.9932 ± 0.0006	0.997^a	NPT
P	bar	79 ± 20		NVT
$\langle \mu \rangle$	D	2.928 ± 0.001	2.9^c	NPT
τ_1^{HH}	ps	5.29 ± 0.06		NVE
τ_2^{HH}	ps	2.35 ± 0.02		NVE
τ_1^{OH}	ps	4.97 ± 0.06		NVE
τ_2^{OH}	ps	2.01 ± 0.02	1.95^d	NVE
D_s	10 ⁻⁵ cm ² /s	1.83 ± 0.02	2.32^e	NVE
$\langle q_{\text{H}}^{\text{perm}} \rangle$	e	0.2055 ± 0.0001		NPT
$\langle q_{\text{H}}^{\text{ind}} \rangle$	e	0.0606 ± 0.0002		NPT
$\langle q_{\text{O}}^{\text{perm}} \rangle$	e	-0.4110 ± 0.0001		NPT
$\langle q_{\text{O}}^{\text{ind}} \rangle$	e	-0.1211 ± 0.0004		NPT

^a Reference 73. ^b Reference 69. ^c Reference 71. ^d Reference 92. ^e Reference 68. ^f The simulations were carried out without the intermolecular interactions. From eight separate runs of 100 ps NVT simulations.

density 0.997 g/cm³.⁷³ It is known that the pressure is very sensitive to the treatment of electrostatic interactions and the system size.⁷⁴ In our simulation, the system size was relatively small and the electrostatic interactions including quadrupoles and the dispersion term were cut off. Therefore, the pressure calculations are not expected to be accurate. The averaged potential energy of liquid water is -9.036 ± 0.006 kcal/mol. Assuming the water vapor is an ideal gas, the heat of vaporization is calculated from

$$\Delta H_{\text{vap}} = -E_{\text{liquid}} + E_{\text{gas}} + RT \quad (26)$$

where E_{liquid} and E_{gas} are the averaged potential energies of water in the liquid and gas phases, respectively, and R is the gas constant. We found $E_{\text{gas}} = 0.900 \pm 0.002$ kcal/mol by carrying out the NVT simulations without the intermolecular interactions. The heat of vaporization ΔH_{vap} for this model is 10.54 ± 0.01 kcal/mol which is in good agreement with the experimentally measured ΔH_{vap} of 10.52 kcal/mol.⁷³

We further computed the rotational relaxation time from the NVE simulations to show the dynamic property of liquid water. The rotational correlation functions are defined as

$$C_n(t) = \left\langle P_n \left(\frac{\mathbf{v}(t) \cdot \mathbf{v}(0)}{|\mathbf{v}(t)| |\mathbf{v}(0)|} \right) \right\rangle \quad (27)$$

where $P_n(x)$ is the n th Legendre polynomial and $\mathbf{v}(t)$ is the vector along the specific molecular axis. We calculated $C_1(t)$ and $C_2(t)$ for the two vector elements, namely, the H–H vector and the O–H vector. The correlation functions were integrated over 50 ps to evaluate the relaxation times. We denote the relaxation times of the H–H and O–H vectors as τ_n^{HH} and τ_n^{OH} , respectively. All the calculated properties are summarized in Table 2.

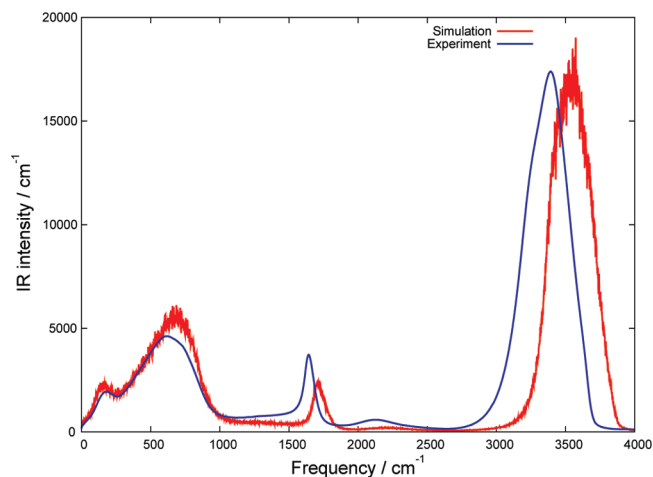


Figure 4. IR spectrum of bulk water at about 300 K. The experimental spectrum is from ref 57.

4. INFRARED SPECTRA

The IR spectra were calculated via the correlation function with the harmonic quantum correction factor given by^{75,76}

$$n(\omega)\alpha(\omega) = \frac{\pi\beta\omega^2}{3cV\epsilon_0} \left(\frac{1}{2\pi} \right) \int_{-\infty}^{\infty} dt e^{-i\omega t} \langle \mathbf{M}(t) \cdot \mathbf{M}(0) \rangle \quad (28)$$

where c , ϵ_0 , $\alpha(\omega)$, and $n(\omega)$ are the speed of light, the vacuum permittivity, the molar absorption coefficient, and the frequency dependent index of refraction. The harmonic quantum correction factor defined by

$$Q_C(\omega) = \frac{\beta\hbar\omega}{(1 - \exp(-\beta\hbar\omega))} \quad (29)$$

works well even for highly anharmonic vibrations.⁷⁷ Figure 4 shows the calculated IR spectrum and the experimental result from Bertie.⁵⁷ The IR spectrum decomposed into the permanent, induced, and their cross contributions are shown in Figure 5. Note that the present model has induced atomic dipoles even without external electric fields because the model has intramolecular dipole–dipole and charge–dipole interactions. Here, the induced contribution is obtained from the total dipole moment of the system minus the monomer dipole moments. The present water model was parametrized to reproduce the intensity of the O–H stretching spectrum. Without the blue shift of the spectral peaks, the line shape and intensity of the spectrum in the region 3000–4000 cm⁻¹ is consistent with the experiment. This difference between this classical MD simulation and the experiment is unavoidable due to a limitation of the classical treatment of the highly anharmonic vibrations based on a quantum mechanical potential.^{76,78} The peak of the calculated OH stretching spectrum is around 3550 cm⁻¹, which is 150 cm⁻¹ higher than the experimental peak position. Such peak shifts can be calibrated in an *ad hoc* manner by rescaling the frequency as $\omega \rightarrow 0.96\omega$. While the rapid decrease of the blue side of the experimental spectrum is well reproduced, the intensity of the red side of the calculated spectrum is slightly weaker than the experimental data. The strong enhancement of the OH-stretching band by local electric fields is observed in Figure 5. The intensity of the OH-stretching band is about 18 times stronger than that of the permanent contribution. The calculated H–O–H bending peak appears at 1700 cm⁻¹ with

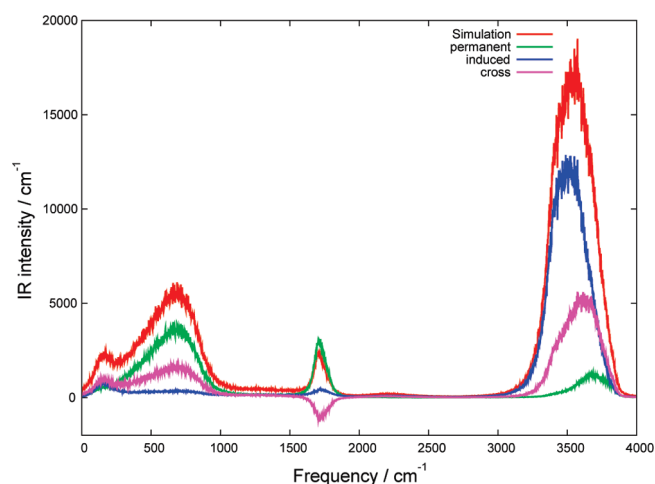


Figure 5. IR spectra of bulk water decomposed into permanent, induced, and permanent-induced cross contributions. The total IR spectrum is also shown for comparison.

the intensity slightly weaker than the experimental result about 60 cm^{-1} higher position. Figure 5 also indicates that the induced dipole contribution slightly weakens the intensity of the bending signal.

In the intermolecular low-frequency region, although the calculated spectrum is slightly stronger in the region from 600 to 900 cm^{-1} , the result is almost consistent with experimental data. The IR spectrum of the presented water model has a prominent peak around 200 cm^{-1} , which comes from the induced dipole component. It has been suggested that the 200 cm^{-1} peak arises from the intermolecular charge fluctuations in the tetrahedral structure.^{21,22} This suggestion is motivated by the fact that, while the empirical force field models have had difficulties reproducing this peak,^{11,38,39} it can be reproduced by AIMD simulations. Because the present water model has no intermolecular charge fluctuation, the present result suggests another possibility for the origin of the 200 cm^{-1} peak.

5. RAMAN SPECTRA

While we chose the interactions and parameters mainly to reproduce experimentally obtained IR spectra, we found that the present model can reproduce Raman spectra reasonably well, especially for high-frequency intramolecular vibrational modes. We calculated the parallel-polarized (VV) and perpendicular-polarized (VH) Raman spectra from the NVE simulations. The isotropic and anisotropic Raman spectra with the harmonic quantum correction factor of the OH stretch region were calculated by^{75,79}

$$I_{\text{iso}}(\omega) = Q_C(\omega) \left(\frac{\lambda(\omega)}{2\pi} \right)^{-4} \frac{1}{2\pi} \int_{-\infty}^{\infty} e^{-i\omega t} \langle \alpha_{\text{iso}}(t) \alpha_{\text{iso}}(0) \rangle dt \quad (30)$$

and

$$I_{\text{aniso}}(\omega) = Q_C(\omega) \left(\frac{\lambda(\omega)}{2\pi} \right)^{-4} \frac{1}{2\pi} \int_{-\infty}^{\infty} e^{-i\omega t} \langle \text{tr}[\beta(t)\beta(0)] \rangle dt \quad (31)$$

where $\lambda(\omega)$ is the wavelength of the scattered radiation. The isotropic polarizability and the anisotropic polarizability are,

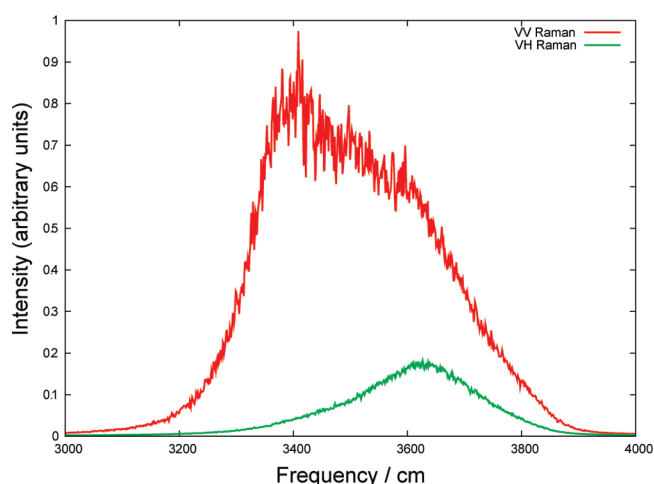


Figure 6. The VV and VH Raman spectra of the OH stretching band of bulk water at about 300 K.

respectively, defined with the polarizability tensor of the system $\mathbf{\Pi}(t)$ by $\alpha_{\text{iso}}(t) = \text{tr}[\mathbf{\Pi}(t)]/3$ and $\beta(t) = \mathbf{\Pi}(t) - \alpha_{\text{iso}}(t)\mathbf{1}$. The VV and VH Raman spectra are then obtained from $I_{\text{VV}}(\omega) = I_{\text{iso}}(\omega) + (2/15)I_{\text{aniso}}(\omega)$ and $I_{\text{VH}}(\omega) = (1/10)I_{\text{aniso}}(\omega)$.⁷⁵ We have used the approximation $\lambda(\omega) = 2\pi c(\omega_0 - \omega)^{-1}$, where c is the speed of the light in a vacuum and ω_0 is the frequency of the incident radiation set by $2\pi c/\omega_0 = 488\text{ nm}$. The calculated Raman spectra of the OH stretching band are shown in Figure 6. The peak of the calculated VH Raman spectrum at 3600 cm^{-1} is experimentally observed at the peak around 3400 cm^{-1} with an unsymmetrical profile. The blue peak shifts of the calculated spectrum are due to the absence of the quantum effect. Like the case of IR, the peak shifts can be calibrated in an *ad hoc* manner by rescaling the frequency as $\omega \rightarrow 0.96\omega$. While the experimental VV Raman spectrum^{58,80} exhibits a broadened peak around $3000\text{--}3800\text{ cm}^{-1}$ with two small bumps at 3200 and 3400 cm^{-1} , the calculated spectrum shows a similar peak around $3200\text{--}3800\text{ cm}^{-1}$ but without the bumps.

The Bose–Einstein (BE) corrected isotropic and anisotropic Raman spectra in the frequency range $0\text{--}2000\text{ cm}^{-1}$ were obtained from $I_{\text{BE}}(\omega) = (1 - \exp(-\beta\hbar\omega))I(\omega)$.⁸¹ The BE corrected Raman spectrum is known to be proportional to the imaginary part of the Fourier transformed optical Kerr effect (OKE) response function.^{82,83} The calculated BE corrected Raman spectra are shown in Figure 7. Experimentally, two distinct peaks at 60 and 180 cm^{-1} and a broad peak at around 500 cm^{-1} were observed in the low-frequency anisotropic spectrum.^{81,83,84} Normal mode analysis of liquid water for intermolecular modes indicated the peaks at about 60 and 200 cm^{-1} correspond to the hindered translational motions of O–O–O bending and O–O stretching of O–H···O, respectively, while the peak above 400 cm^{-1} corresponds to the librational motion of water molecules.^{85–87} The calculated BE corrected anisotropic Raman spectrum shows a single distinct peak corresponding to O–O stretching at 200 cm^{-1} . On the contrary to the anisotropic case, the isotropic spectrum exhibits a prominent peak at around 60 cm^{-1} in addition to the broad peak at around 800 cm^{-1} . We may enhance the anisotropic and isotropic polarizability elements to adjust the peak at 60 cm^{-1} and the peak above 400 cm^{-1} in the anisotropic and isotropic spectra. To this end, the dipole induced-dipole treatment of the

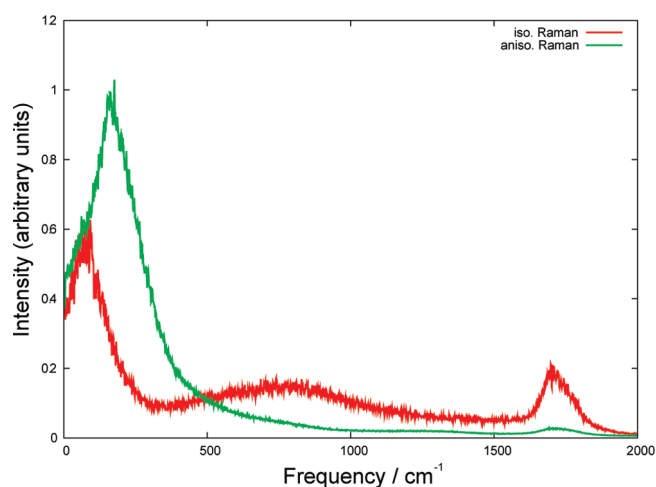


Figure 7. The BE corrected isotropic and anisotropic Raman spectra of the low-frequency region of bulk water at about 300 K. Here, the intensity of the isotropic spectrum is magnified by a factor of 1.5.

polarizability may be extended.⁸⁴ However, such treatments may alter the IR spectral profile in the low-frequency range. The form of the harmonic quantum correction factor may also be modified, since the low-frequency intermolecular modes may not be an ensemble of harmonic modes but damped anharmonic modes. Further experimental results, such as multidimensional Raman^{41,88} and/or THz^{89,90} spectra, are necessary to identify the problem. Because of this, we have not altered the spectra with any of these methods.

6. CONCLUSIONS

We developed a polarizable water potential model for inter- and intramolecular vibrational spectra. This model is based on the POLIR potential model⁴⁰ with atomic multipoles up to quadrupoles and the charge and dipole polarizabilities included. The polarization effects and dipole moment surface are consistently parametrized by the distributed multipole analysis.^{55,56} The bulk properties under ambient conditions are quantitatively in good agreement with the experimental data except for the self-diffusion coefficient. The present model can reproduce the line shape and intensity of the OH stretching band and the intermolecular IR spectrum, while the model predicts the slightly weaker HOH bending band. Although charge fluctuations between the molecules were not implemented in the present water model, we still obtain the distinct peak at 200 cm⁻¹ in the IR spectrum, which was thought to arise from the intermolecular charge fluctuation,^{21,22} indicating another possibility for a cause of this peak.

In the low-frequency anisotropic Raman spectrum, the absence of the peak at around 60 cm⁻¹, which corresponds to the hydrogen bond bending mode, was observed. The peak above 400 cm⁻¹ corresponding to the librational modes is also different from the experimental results. While we have difficulty in reproducing the low-frequency depolarized Raman spectrum, we leave the adjustment of our model to low-frequency Raman modes for future study. There are too many possibilities for the cause of this discrepancy at this stage.

The differences of the vibrational spectra between the different potential models are not easy to see in the linear IR and third-order Raman responses, and we expect that such differences will

be enhanced in multidimensional vibrational spectroscopies.⁵⁴ Since higher-order spectroscopy, such as fifth-order Raman⁴¹ and third-order IR spectroscopy,⁴² measures the vibrational relaxation process with more than two successive pumping processes, we are able to disentangle a role of interactions between the atoms as well as molecules in more detail.^{4,49} In a future study, we will explore the interplay between inter- and intramolecular vibrations by monitoring multidimensional vibrational spectra calculated from full MD simulations^{50,91} using the present potential model.

APPENDIX

We used the switching function of the distance of the center of mass written as

$$f(R_{ij}) = \frac{(R_{ij} - R_{C2})^3 (10R_{C1}^2 + R_{C2}^2 + 3R_{C2}R_{ij} + 6R_{ij}^2 - 5R_{C1}(R_{C2} + 3R_{ij}))}{(R_{C1} - R_{C2})^5} \quad (\text{A1})$$

where R_{ij} is the distance of the center of mass between molecule i and j , R_{C1} and R_{C2} are the cutoff parameters. The values of this function decrease from 1 at R_{C1} to zero at R_{C2} .

ASSOCIATED CONTENT

S Supporting Information. Tables showing the parameters for potential charge, permanent dipole, unit vector of dipole moment, quadrupole, charge polarizability, and dipole polarizability. This material is available free of charge via the Internet at <http://pubs.acs.org>.

ACKNOWLEDGMENT

We thank Prof. S. Saito and Dr. Y. Nagata for fruitful discussions. Y.T. is thankful for the financial support from a Grant-in-Aid for Scientific Research B19350011 from the Japan Society for the Promotion of Science. T.H. appreciates the support of Research Fellowships of the Japan Society for the Promotion of Science. This work was supported by the Grant-in-Aid for JSPS Fellows 21·961 from the JSPS. A part of the computations was performed at Research Center for Computational Science, Okazaki, Japan.

REFERENCES

- (1) Mukamel, S. *Principles of Nonlinear Optical Spectroscopy*; Oxford University Press: New York, 1995.
- (2) Eisenberg, D.; Kauzmann, W. *The Structure and Properties of Water*; Oxford University Press: New York, 1969.
- (3) Madden, P. A.; Impey, R. W. *Chem. Phys. Lett.* **1986**, *123*, 502.
- (4) Yagasaki, T.; Ono, J.; Saito, S. *J. Chem. Phys.* **2009**, *131*, 164511.
- (5) Iftimie, R.; Tuckerman, M. E. *J. Chem. Phys.* **2005**, *122*, 214508.
- (6) Bursulaya, B. D.; Kim, H. J. *J. Chem. Phys.* **1998**, *109*, 4911.
- (7) Yang, M.; Skinner, J. L. *Phys. Chem. Chem. Phys.* **2010**, *12*, 982.
- (8) Bakker, H. J.; Skinner, J. L. *Chem. Rev.* **2010**, *110*, 1498.
- (9) Torii, H. *J. Phys. Chem. A* **2006**, *110*, 9469.
- (10) Ahlborn, H.; Space, B.; Moore, P. B. *J. Chem. Phys.* **2000**, *112*, 8083.
- (11) Ahlborn, H.; Ji, X. D.; Space, B.; Moore, P. B. *J. Chem. Phys.* **1999**, *111*, 10622.
- (12) Auer, B. M.; Skinner, J. L. *J. Chem. Phys.* **2008**, *128*, 224511.

- (13) Habershon, S.; Markland, T. E.; Manolopoulos, D. E. *J. Chem. Phys.* **2009**, *131*, 024501.
- (14) Kraemer, D.; Cowan, M. L.; Paarmann, A.; Huse, N.; Nibbering, E. T. J.; Elsaesser, T.; Miller, R. J. D. *Proc. Natl. Acad. Sci. U.S.A.* **2008**, *105*, 437.
- (15) Paarmann, A.; Hayashi, T.; Mukamel, S.; Miller, R. J. D. *J. Chem. Phys.* **2008**, *128*, 191103.
- (16) Paarmann, A.; Hayashi, T.; Mukamel, S.; Miller, R. J. D. *J. Chem. Phys.* **2009**, *130*, 204110.
- (17) Cowan, M. L.; Bruner, B. D.; Huse, N.; Dwyer, J. R.; Chugh, B.; Nibbering, E. T. J.; Elsaesser, T.; Miller, R. J. D. *Nature* **2005**, *434*, 199.
- (18) Car, R.; Parrinello, M. *Phys. Rev. Lett.* **1985**, *55*, 2471.
- (19) Silvestrelli, P. L.; Parrinello, M. *J. Chem. Phys.* **1999**, *111*, 3572.
- (20) Lee, H. S.; Tuckerman, M. E. *J. Chem. Phys.* **2007**, *126*, 164501.
- (21) Sharma, M.; Resta, R.; Car, R. *Phys. Rev. Lett.* **2005**, *95*, 187401.
- (22) Heyden, M.; Sun, J.; Funkner, S.; Mathias, G.; Forbert, H.; Havenith, M.; Marx, D. *Proc. Natl. Acad. Sci. U.S.A.* **2010**, *107*, 12068.
- (23) Silvestrelli, P. L.; Bernasconi, M.; Parrinello, M. *Chem. Phys. Lett.* **1997**, *277*, 478.
- (24) Mukamel, S.; Tanimura, Y.; Hamm, P. *Acc. Chem. Res.* **2009**, *42*, 1207.
- (25) Rappe, A. K.; Goddard, W. A. *J. Phys. Chem.* **1991**, *95*, 3358.
- (26) Rick, S. W.; Stuart, S. J.; Berne, B. J. *J. Chem. Phys.* **1994**, *101*, 6141.
- (27) Nagata, Y.; Mukamel, S. *J. Am. Chem. Soc.* **2010**, *132*, 6434.
- (28) Applequi, J.; Carl, J. R.; Fung, K. K. *J. Am. Chem. Soc.* **1972**, *94*, 2952.
- (29) Thole, B. T. *Chem. Phys.* **1981**, *59*, 341.
- (30) Morita, A.; Kato, S. *J. Am. Chem. Soc.* **1997**, *119*, 4021.
- (31) Morita, A.; Kato, S. *J. Chem. Phys.* **1998**, *108*, 6809.
- (32) Ishiyama, T.; Morita, A. *J. Chem. Phys.* **2009**, *131*, 244714.
- (33) Guillot, B. *J. Mol. Liq.* **2002**, *101*, 219.
- (34) Stern, H. A.; Rittner, F.; Berne, B. J.; Friesner, R. A. *J. Chem. Phys.* **2001**, *115*, 2237.
- (35) Ren, P. Y.; Ponder, J. W. *J. Phys. Chem. B* **2004**, *108*, 13427.
- (36) Ren, P. Y.; Ponder, J. W. *J. Phys. Chem. B* **2003**, *107*, 5933.
- (37) Partridge, H.; Schwenke, D. W. *J. Chem. Phys.* **1997**, *106*, 4618.
- (38) Fanourgakis, G. S.; Xantheas, S. S. *J. Chem. Phys.* **2008**, *128*, 074506.
- (39) Burnham, C. J.; Anick, D. J.; Mankoo, P. K.; Reiter, G. F. *J. Chem. Phys.* **2008**, *128*, 154519.
- (40) Mankoo, P. K.; Keyes, T. J. *J. Chem. Phys.* **2008**, *129*, 034504.
- (41) Tanimura, Y.; Mukamel, S. *J. Chem. Phys.* **1993**, *99*, 9496.
- (42) Hamm, P.; Lim, M. H.; Hochstrasser, R. M. *J. Phys. Chem. B* **1998**, *102*, 6123.
- (43) Yagasaki, T.; Saito, S. *J. Chem. Phys.* **2008**, *128*, 154521.
- (44) Evans, D. J.; Gaylor, K. *Mol. Phys.* **1983**, *49*, 963.
- (45) Jansen, T. L. C.; Snijders, J. G.; Duppen, K. *J. Chem. Phys.* **2000**, *113*, 307.
- (46) Ma, A.; Stratt, R. M. *J. Chem. Phys.* **2002**, *116*, 4962.
- (47) Everitt, K. F.; Geva, E.; Skinner, J. L. *J. Chem. Phys.* **2001**, *114*, 1326.
- (48) Hasegawa, T.; Tanimura, Y. *J. Chem. Phys.* **2006**, *125*, 074512.
- (49) Tanimura, Y.; Ishizaki, A. *Acc. Chem. Res.* **2009**, *42*, 1270.
- (50) Hasegawa, T.; Tanimura, Y. *J. Chem. Phys.* **2008**, *128*, 064511.
- (51) Saito, S.; Ohmine, I. *J. Chem. Phys.* **1997**, *106*, 4889.
- (52) Saito, S.; Ohmine, I. *J. Chem. Phys.* **1995**, *102*, 3566.
- (53) Yagasaki, T.; Saito, S. *Acc. Chem. Res.* **2009**, *42*, 1250.
- (54) Li, Y. L.; Huang, L.; Miller, R. J. D.; Hasegawa, T.; Tanimura, Y. *J. Chem. Phys.* **2008**, *128*, 234507.
- (55) Stone, A. J.; Alderton, M. *Mol. Phys.* **1985**, *56*, 1047.
- (56) Stone, A. J. *Mol. Phys.* **1985**, *56*, 1065.
- (57) Bertie, J. E.; Lan, Z. D. *Appl. Spectrosc.* **1996**, *50*, 1047.
- (58) Walrafen, G. E.; Hokmabadi, M. S.; Yang, W. H. *J. Chem. Phys.* **1986**, *85*, 6964.
- (59) Buckingham, A. D. *Q. Rev. Chem. Soc.* **1959**, *13*, 183.
- (60) Ahlstrom, P.; Wallqvist, A.; Engstrom, S.; Jonsson, B. *Mol. Phys.* **1989**, *68*, 563.
- (61) Halgren, T. A. *J. Am. Chem. Soc.* **1992**, *114*, 7827.
- (62) Frisch, M. J.; Trucks, G. W.; Schlegel, H. B.; Scuseria, G. E.; Robb, M. A.; Cheeseman, J. R.; Montgomery, J. A.; Vreven, T.; Kudin, K. N.; Burant, J. C.; Millam, J. M.; Iyengar, S. S.; Tomasi, J.; Barone, V.; Mennucci, B.; Cossi, M.; Scalmani, G.; Rega, N.; Petersson, G. A.; Nakatsuji, H.; Hada, M.; Ehara, M.; Toyota, K.; Fukuda, R.; Hasegawa, J.; Ishida, M.; Nakajima, T.; Honda, Y.; Kitao, O.; Nakai, H.; Klene, M.; Li, X.; Knox, J. E.; Hratchian, H. P.; Cross, J. B.; Bakken, V.; Adamo, C.; Jaramillo, J.; Gomperts, R.; Stratmann, R. E.; Yazyev, O.; Austin, A. J.; Cammi, R.; Pomelli, C.; Ochterski, J. W.; Ayala, P. Y.; Morokuma, K.; Voth, G. A.; Salvador, P.; Dannenberg, J. J.; Zakrzewski, V. G.; Dapprich, S.; Daniels, A. D.; Strain, M. C.; Farkas, O.; Malick, D. K.; Rabuck, A. D.; Raghavachari, K.; Foresman, J. B.; Ortiz, J. V.; Cui, Q.; Baboul, A. G.; Clifford, S.; Cioslowski, J.; Stefanov, B. B.; Liu, G.; Liashenko, A.; Piskorz, P.; Komaromi, I.; Martin, R. L.; Fox, D. J.; Keith, T.; Laham, A.; Peng, C. Y.; Nanayakkara, A.; Challacombe, M.; Gill, P. M. W.; Johnson, B.; Chen, W.; Wong, M. W.; Gonzalez, C.; Pople, J. A. *Gaussian 03*, revision E.01; Gaussian, Inc.: Wallingford, CT, 2003.
- (63) Burnham, C. J.; Li, J.; Xantheas, S. S.; Leslie, M. J. *Chem. Phys.* **1999**, *110*, 4566.
- (64) Martyna, G. J.; Tuckerman, M. E.; Tobias, D. J.; Klein, M. L. *Mol. Phys.* **1996**, *87*, 1117.
- (65) Tuckerman, M.; Berne, B. J.; Martyna, G. J. *J. Chem. Phys.* **1992**, *97*, 1990.
- (66) Berendsen, H. J. C.; Grigera, J. R.; Straatsma, T. P. *J. Phys. Chem.* **1987**, *91*, 6269.
- (67) Soper, A. K. *Chem. Phys.* **2000**, *258*, 121.
- (68) Krynicki, K.; Green, C. D.; Sawyer, D. W. *Faraday Discuss.* **1978**, *66*, 199.
- (69) Ichikawa, K.; Kameda, Y.; Yamaguchi, T.; Wakita, H.; Misawa, M. *Mol. Phys.* **1991**, *73*, 79.
- (70) Burnham, C. J.; Xantheas, S. S. *J. Chem. Phys.* **2002**, *116*, 5115.
- (71) Badyal, Y. S.; Saboungi, M. L.; Price, D. L.; Shastri, S. D.; Haefner, D. R.; Soper, A. K. *J. Chem. Phys.* **2000**, *112*, 9206.
- (72) Delle Site, L.; Alavi, A.; Lynden-Bell, R. M. *Mol. Phys.* **1999**, *96*, 1683.
- (73) Wagner, W.; Pruss, A. *J. Phys. Chem. Ref. Data* **2002**, *31*, 387.
- (74) Hummer, G.; Gronbech-Jensen, N.; Neumann, M. *J. Chem. Phys.* **1998**, *109*, 2791.
- (75) McQuarrie, D. A. *Statistical Mechanics*; Harper and Row: New York, 1976.
- (76) Berens, P. H.; Wilson, K. R. *J. Chem. Phys.* **1981**, *74*, 4872.
- (77) Ramirez, R.; Lopez-Ciudad, T.; Kumar, P.; Marx, D. *J. Chem. Phys.* **2004**, *121*, 3973.
- (78) Sakurai, A.; Tanimura, Y. *J. Phys. Chem. A* [Online early access]. DOI: 10.1021/jp1095618. Published Online: Jan 19, 2011.
- (79) Berens, P. H.; White, S. R.; Wilson, K. R. *J. Chem. Phys.* **1981**, *75*, 515.
- (80) Murphy, W. F.; Bernstein, H. J. *J. Phys. Chem.* **1972**, *76*, 1147.
- (81) Walrafen, G. E.; Fisher, M. R.; Hokmabadi, M. S.; Yang, W. H. *J. Chem. Phys.* **1986**, *85*, 6970.
- (82) Ji, X. D.; Ahlborn, H.; Space, B.; Moore, P. B. *J. Chem. Phys.* **2000**, *113*, 8693.
- (83) Castner, E. W.; Chang, Y. J.; Chu, Y. C.; Walrafen, G. E. *J. Chem. Phys.* **1995**, *102*, 653.
- (84) Fecko, C. J.; Eaves, J. D.; Tokmakoff, A. *J. Chem. Phys.* **2002**, *117*, 1139.
- (85) Ohmine, I.; Saito, S. *Acc. Chem. Res.* **1999**, *32*, 741.
- (86) Cho, M.; Fleming, G. R.; Saito, S.; Ohmine, I.; Stratt, R. M. *J. Chem. Phys.* **1994**, *100*, 6672.
- (87) Ohmine, I.; Tanaka, H. *Chem. Rev.* **1993**, *93*, 2545.
- (88) Saito, S.; Ohmine, I. *J. Chem. Phys.* **2006**, *125*, 084506.
- (89) Okumura, K.; Tanimura, Y. *Chem. Phys. Lett.* **1998**, *295*, 298.
- (90) Hattori, T. *J. Chem. Phys.* **2010**, *133*, 204503.
- (91) Jeon, J.; Cho, M. *New J. Phys.* **2010**, *12*, 065001.
- (92) Ludwig, R. *Chem. Phys.* **1995**, *195*, 329.